

Journal of Materials Chemistry C

Accepted Manuscript



This is an *Accepted Manuscript*, which has been through the Royal Society of Chemistry peer review process and has been accepted for publication.

Accepted Manuscripts are published online shortly after acceptance, before technical editing, formatting and proof reading. Using this free service, authors can make their results available to the community, in citable form, before we publish the edited article. We will replace this *Accepted Manuscript* with the edited and formatted *Advance Article* as soon as it is available.

You can find more information about *Accepted Manuscripts* in the [Information for Authors](#).

Please note that technical editing may introduce minor changes to the text and/or graphics, which may alter content. The journal's standard [Terms & Conditions](#) and the [Ethical guidelines](#) still apply. In no event shall the Royal Society of Chemistry be held responsible for any errors or omissions in this *Accepted Manuscript* or any consequences arising from the use of any information it contains.

The table of contents entry

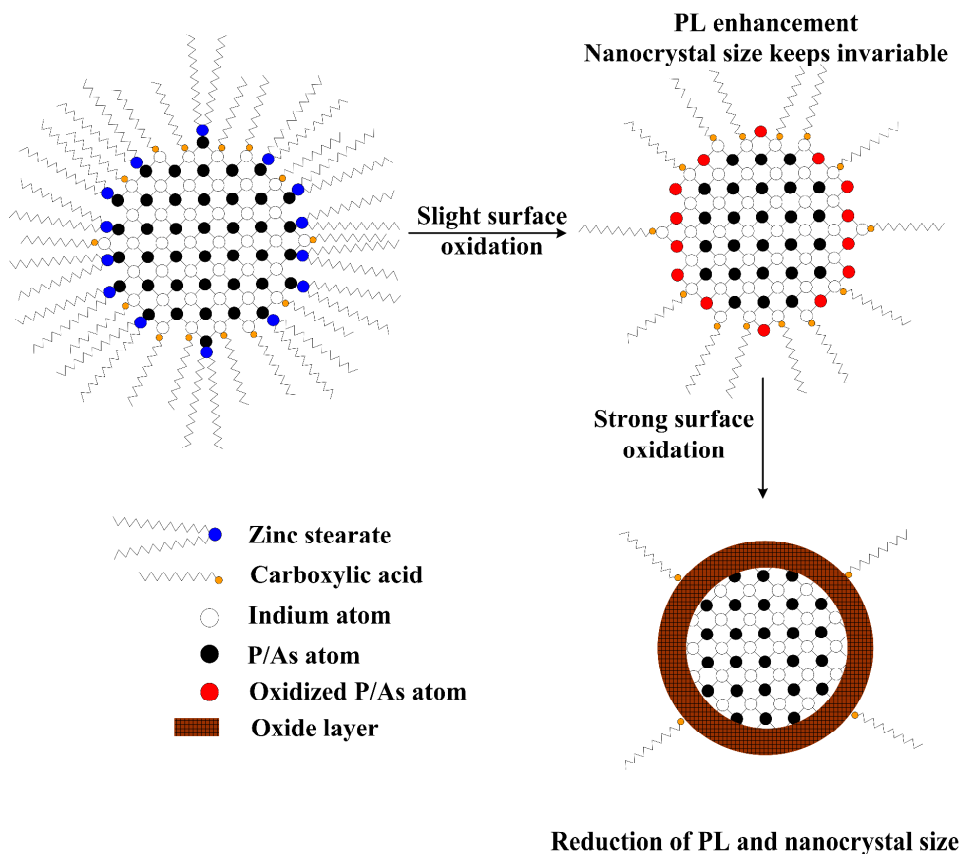
Surface oxidation substantially affects the optical property of nanocrystals. Primary oxidation eliminates the surface dangling bonds and leads to PL enhancement while does not affect the nanocrystal size. However, further surface oxidation forms a coarse oxide layer which results in reduction in PL and nanocrystal size.

Keyword: InP Nanocrystals; InAs Nanocrystals; Core/Shell Nanoparticles; Photoluminescence; Quantum Yield; Optical Stability

Jianbing Zhang,^{a, b} Rong Li,^a Weipeng Sun,^a Qi Wang,^a Xiangshui Miao,^{a, b} and Daoli Zhang^{a, b, *}

Temporal evolutions of the photoluminescence quantum yields of colloidal InP, InAs and their core/shell nanocrystals

ToC figure



Temporal evolutions of the photoluminescence quantum yields of colloidal InP, InAs and their core/shell nanocrystals

Cite this: DOI: 10.1039/x0xx00000x

Received 10th March 2014,
Accepted 00th January 2012

DOI: 10.1039/x0xx00000x

www.rsc.org/

Jianbing Zhang,^{a, b} Rong Li,^a Weipeng Sun,^a Qi Wang,^a Xiangshui Miao,^{a, b} and Daoli Zhang^{a, b, *}

Colloidal InP, InAs and their core/shell nanocrystals are synthesized using *in situ* generated PH₃ and AsH₃, respectively, and the optical stability of these nanocrystals is studied by monitoring the absorption and photoluminescence spectra. The quantum yield or photoluminescence intensity of InP nanocrystals synthesized in the presence of zinc stearate increases monotonously from 3% to 16% while the photoluminescence peak position keeps invariable during the storage 30 days in the hexane solvent and in the dark. On the contrary, InAs nanocrystals synthesized in the presence of or in the absence of zinc stearate lose their photoluminescence gradually and show the reduction of their size during the storage. For the core/shell nanocrystals, InP/ZnS nanocrystals exhibit the fine optical stability in the first few days and a little decrease in the photoluminescence quantum yield from 15 to 30 days. InAs/ZnSe nanocrystals with the different shell thickness show monotonous increase in the quantum yield and blue-shift in the photoluminescence peak in the course of 30 days. Despite two shells, InAs/ZnSe/ZnS nanocrystals are still sensitive to surface states. The experiments show slight surface oxidation eliminates dangling bonds and leads to enhancement of photoluminescence. Strong oxidation results in the formation of an oxide layer on the nanocrystal surface, giving rise to the reduction of photoluminescence.

1. Introduction

Colloidal semiconductor nanocrystals have excellent optical properties, such as composition- and size-tunable emission, high photoluminescence quantum yield (QY), broad range of excitation wavelength, good stability compared to organic dyes, long luminescent lifetime, et. al. Hence they are promising luminescent materials which can be used in light emitting diode,¹⁻⁴ laser,^{5, 6} telecommunication^{7, 8} and especially in biological applications.^{9, 10} The QY and stability of the nanocrystals are key important for their applications, and there are some literatures concerning about the

photoactivation of II-VI and IV-VI nanocrystals dissolved in organic solvents or water.¹¹⁻¹⁵ The observations show the enhancement of photoluminescence (PL) intensity under irradiation and reduction of the PL intensity under longer irradiation in atmospheres containing O₂ or H₂O.¹⁶ Recently, Yu and co-workers¹⁷ systematically studied the optical stability of PbSe nanocrystals. They also observed the PL intensity increased first and then decreased slowly under ultraviolet (UV) exposure in air. Nevertheless, no systematic study was reported on the optical stability of III-V colloidal nanocrystals in the existing literatures. These nanocrystals have larger exciton radii, lower toxicity than Cd- and Pb-containing nanocrystals, and the emission of them covers visible and infrared windows which are suitable for applications in biological and telecommunication.^{18, 19} Moreover, III-V nanocrystals may show different optical stability from II-VI and IV-VI nanocrystals due to different chemical properties.

In order to improve QY and optical stability, shells with broader band gap are epitaxially coated on core nanocrystals. It is expected that the core/shell nanocrystals have excellent stability, but there is a lack of sufficient experimental observations. In the previous work,²⁰ we demonstrated that InP or InAs nanocrystals with well-controlled size and size distribution could be formed using

^a School of Optical and Electronic Information, Huazhong University of Science and Technology, No. 1037 Luoyu Road, Hongshan District, Wuhan City, Hubei Province, 430074, P. R. China. Electronic mail: zhang_daoli@hust.edu.cn

^b Wuhan National Laboratory for Optoelectronics, 1037 Luoyu Road, Hongshan District, Wuhan City, Hubei Province, 430074, P. R. China

† Electronic Supplementary Information (ESI) available: Absorption and PL spectra of InP, InAs and their core/shell nanocrystals in the one-pot synthesis and XRD pattern of InP/ZnS core/shell nanocrystals. See DOI: 10.1039/b000000x/

in situ generated PH_3 or AsH_3 as phosphorus or arsenic precursor. In this present paper, we synthesized InP, InAs and their core/shell nanocrystals using *in situ* generated PH_3 or AsH_3 respectively and studied the temporal evolutions of the optical stability and quantum yields of these nanocrystals dispersed in hexane in ambience by monitoring the absorption and photoluminescence spectra systematically.

2. Materials and Methods

2.1 Chemicals.

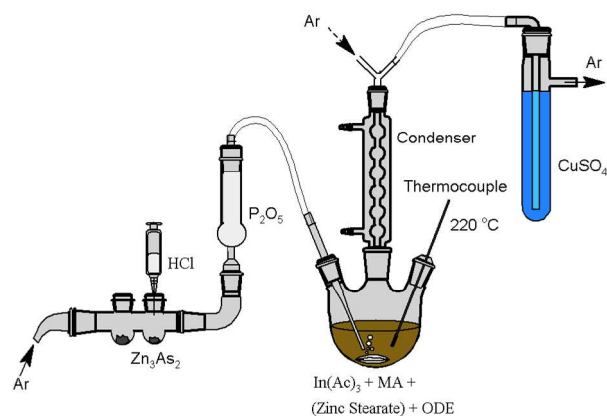
Indium acetate (InAc_3 , 99.99%), calcium phosphide (Ca_3P_2 , 97%), zinc arsenide (Zn_3As_2 , 99%), myristic acid (MA, 98%), 1-octadecene (ODE, 90%), trioctylphosphine (TOP, 90%) and zinc stearate (ZnO 12.5 – 14%) were purchased from Alfa Aesar. Dodecanethiol (DDT, $\geq 98\%$) and Se powder (99.95%) were purchased from Sinopharm Chemical Reagent Co., Ltd. All the chemicals were used as received. PH_3 or AsH_3 generated from the reaction between Ca_3P_2 (or Zn_3As_2) and HCl was used as the phosphorus (or arsenic) sources. The PH_3 or AsH_3 , which are very toxic, should be handled carefully and dried prior to use.

2.2 Synthesis of InAs, InAs/ZnSe and InAs/ZnSe/ZnS nanocrystals.

InAs nanocrystals were synthesized according to ref [20]. Typically, 0.3 mmol InAc_3 was mixed with 0.9 mmol MA and 8 mL ODE in a three neck flask. The mixture was flushed with Ar, and was heated to 220 °C under Ar atmosphere. In another container, 0.15 mmol Zn_3As_2 powder was divided into two parts (0.05 and 0.1 mmol). Firstly, the 0.05 mmol Zn_3As_2 reacted with HCl, about 10 min later, excess HCl was injected into the 0.1 mmol partition. Then the generated AsH_3 was bubbled into the hot indium precursor under Ar flow through a drying tube containing P_2O_5 . The growth of InAs nanocrystals was controlled in 20–30 min. InAs-zinc stearate nanocrystals were synthesized similarly except 0.3 mmol zinc stearate was added along with In source. For the growth of ZnSe shell, the temperature of the reaction solution was dropped down to ~ 130 °C after the formation of InAs-zinc stearate nanocrystals, then 0.3 mL 1 M TOPSe (Se powder dissolved in trioctylphosphine) was added. After that, the reaction mixture was heated to 220 °C very slowly, and maintained at the temperature for 1 hour. For the synthesis of InAs/ZnSe/ZnS nanocrystals, InAs-zinc stearate nanocrystals were synthesized at 240 °C in the presence of 0.6 mmol zinc stearate. Then a layer of ZnSe shell was formed according to the above method. And then a ZnS shell was formed using the same method with that of ZnSe shell except dodecanethiol (DDT) was used as S source. After the formation of these nanocrystals, 0.3 mL reaction product of InAs, InAs-zinc stearate, InAs/ZnSe or InAs/ZnSe/ZnS nanocrystals was dissolved in 5 mL hexane to give clear solutions stored in 7 mL vials, which were loosely capped, in the dark. The absorption and PL spectra of the nanocrystal solutions were recorded at different times to monitor the evolution of optical property. The experimental setup for the synthesis of InAs nanocrystals is schematically shown in Scheme 1.

2.3 Synthesis of InP and InP/ZnS nanocrystals.

Colloidal InP-zinc stearate nanocrystals were synthesized at 250 °C using the same method with that of InAs-zinc stearate



Scheme 1 Experimental setup for the synthesis of InAs nanocrystals.

nanocrystals while Ca_3P_2 is used as phosphorus source which was not divided into two parts. InP/ZnS nanocrystals were synthesized using the same method with that of InAs/ZnSe nanocrystals except the TOPSe was replaced by DDT. Analogously, 0.5 mL of the reaction solution was removed and dissolved in 4 mL hexane after the formation of InP-zinc stearate or InP/ZnS nanocrystals. The absorption and photoluminescence spectra of the nanocrystal solutions, which were in 7 vials with the lid capped loosely, were recorded at different times to monitor the evolution of optical property.

2.4 Characterization of Colloidal InP, InAs and Their Core/Shell Nanocrystals.

Absorption and photoluminescence spectra were measured on a Perkin-Elmer Lambda 35 UV-vis spectrometer and a Jasco FP-6500 fluorescent spectrometer respectively. The quantum yields of the nanocrystals were estimated by comparison with ethanol solution of Rhodamin 6G. QYs at 0 day were obtained by comparing the integrated emission spectra of nanocrystals to those of standard dyes, and then the QYs at the following times were obtained relative to 0 day. Powder X-ray diffraction (XRD) patterns were collected on a PANalytical X'Pert PRO. Transmission electron microscopy (TEM) images were obtained on a FEI Tecnai G2 20 transmission electron microscope operating at an accelerating voltage of 200 kV. Generally, colloidal nanocrystals have low adhesion to the carbon-coated copper grid, so a moderate amount of alcohol was added into the nanocrystals dispersing solution prior to the deposition of the nanocrystals on the carbon-coated copper grid.

3. Results and Discussion

The typical TEM images of colloidal InP, InAs and their core/shell nanocrystals are shown in Figure 1. The nanocrystals are dispersed, separated particles showing little agglomeration and no fusing, and they are roughly spherical. The average sizes of InP and InAs nanocrystals are 4.0 and 1.9 nm respectively.

Figure 2 illustrates the temporal evolutions of absorption and PL spectra, PL full width at half-maximum (FWHM) and QY of InP nanocrystals synthesized in the presence of zinc stearate (InP-zinc stearate). During the 30 days of storage, the

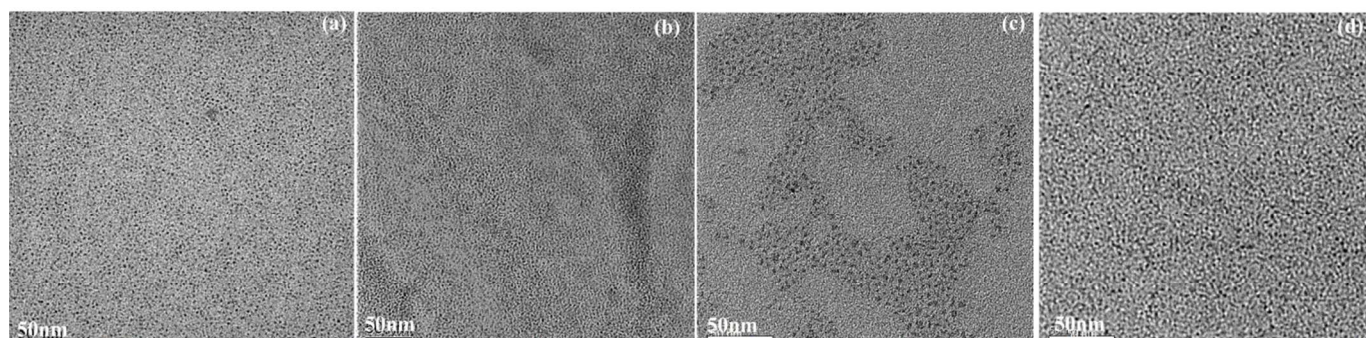


Figure 1. TEM images of colloidal InP (a), InAs (b), InAs/ZnS (c), and InAs/ZnSe (d) nanocrystals. The average sizes of InP and InAs nanocrystals are 4.0 and 1.9 nm respectively.

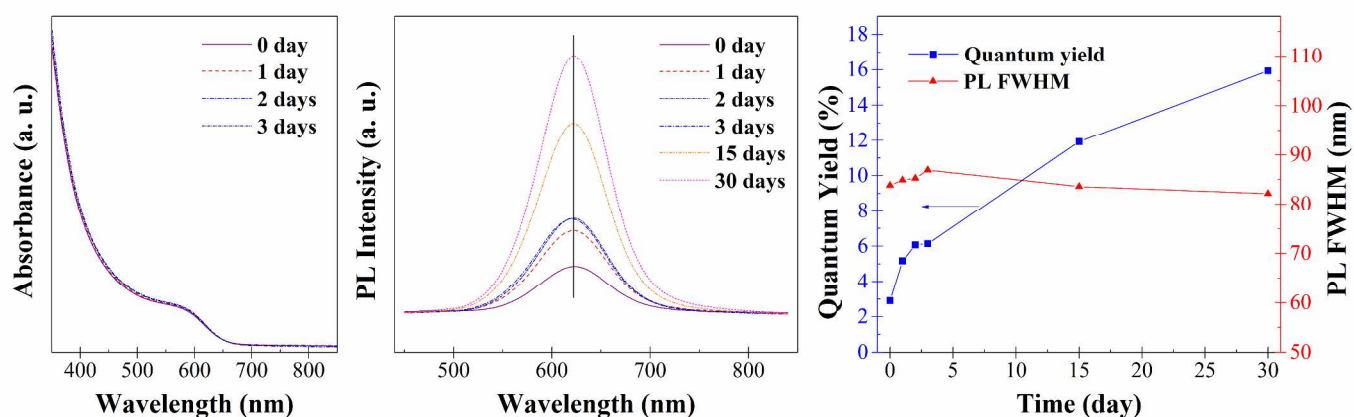


Figure 2. Temporal evolutions of absorption (left) and photoluminescence spectra (middle), photoluminescence FWHM and quantum yield (right) of InP-zinc stearate nanocrystals.

PL intensity increased gradually while the peak position kept invariable, and the QY increased from 3% to 16% while the FWHM varied slightly, indicating that the nanocrystals maintain their size distributions. The fine stability of absorption spectrum in the first 3 days confirmed the invariability of the PL peak position. The enhancement of PL intensity is in accordance with previous observations^{11, 21} which are due to elimination of dangling bonds by surface oxidation, and this kind of oxidation does not affect the particle size.

The addition of zinc stearate is critical for the PL property of InP nanocrystals, which will not show PL if no zinc stearate was added in the synthesis. This can be attributed to zinc stearate which can coordinate to P sites on the surface to provide better passivation without the lattice doping.²²⁻²⁵ However, this coordinate bond is weak, and it will be broken by oxidation of P, which leads to deposition of zinc stearate. This is confirmed by experimental observations that white deposition was observed in the first several days, and the deposition began to emerge near the upper surface of the nanocrystal solution. The process of breaking the P-zinc stearate bonds is also the process of passivating the surface dangling P bonds, while the Indium sites are strongly coordinated by carboxylic acid.

The evolutions of InAs nanocrystals are shown in Figure 3. The InAs nanocrystals synthesized in (InAs-zinc stearate) and without

the presence of zinc stearate showed similar evolutions. The absorption spectra lost their features gradually, the PL intensity and QY decreased substantially. Both the absorption and PL peaks showed pronounced blue-shift, which indicated the InAs core became smaller and lost their PL gradually. During the storage of 30 days, the InAs nanocrystal solution generated brown deposition when it was stored for about 10 days after the deposition of zinc stearate in the first few days. The brown deposition implied the deposition of InAs nanocrystals which may be due to the removal of carboxylic acid by the oxidation of In sites. These demonstrated that the As-zinc stearate bonds were broken first and the In-carboxylic acid bonds would be broken by a strong surface oxidation, and the latter would lead to deposition of nanocrystals.

Comparing with InP nanocrystals, InAs nanocrystals show dramatically different evolutions in QY and PL intensity. This is due to different chemical properties of InAs and InP which determined the rate of surface oxidation. Thus, during the storage of 30 days, the surface oxidation not only eliminated the dangling bonds but also formed an oxide layer on the surface of InAs nanocrystals, resulted in smaller InAs core and lower QY, while the slight surface oxidation only eliminated the dangling bonds and led to increase in QY of InP nanocrystals. The process of surface oxidation is schematically shown in Figure 4.

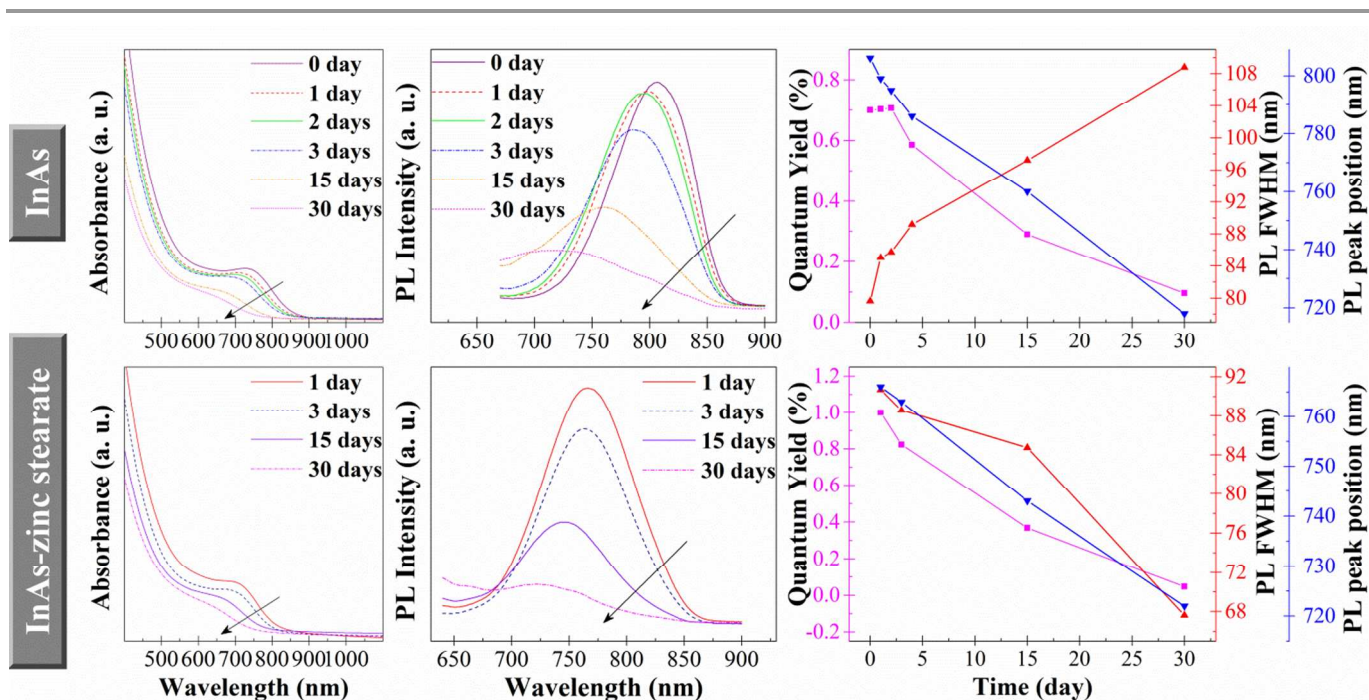


Figure 3. Temporal evolutions of absorption (left) and photoluminescence spectra (middle), quantum yield (■), photoluminescence FWHM (▲) and photoluminescence peak position (▼) (right) of colloidal InAs nanocrystals. (Top row: InAs nanocrystals; bottom row: InAs-zinc stearate nanocrystals)

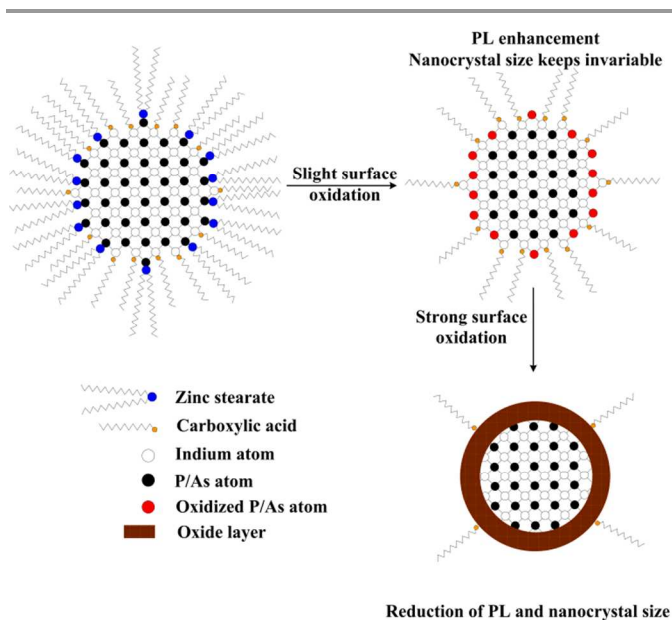


Figure 4. Schematic process of surface oxidation of nanocrystals. Slight surface oxidation breaks the P- or As-zinc stearate bonds and eliminates the dangling bonds, consequently the quantum yield/photoluminescence increases while the nanocrystal size is not affected. Strong surface oxidation forms an oxide layer and results in reduction of quantum yield / photoluminescence and nanocrystal size.

In order to improve the optical properties of core nanocrystals, we synthesized different core/shell nanocrystals, including InP/ZnS, InAs/ZnSe and InAs/ZnSe/ZnS, and studied their optical stability. It

should be mentioned that all of the nanocrystal solutions generated white (zinc stearate) deposition in the first few days when they were stored in hexane. Figure 5 shows the evolutions of InP/ZnS nanocrystals. The absorption and PL spectra kept constant in the first 3 days, indicating excellent stability. However, the PL intensity and QY at the 15th and 30th days decreased a little which can be attributed to formation of the an oxide layer caused by the strong surface oxidation. This implies the elimination of dangling bonds caused by the slight surface oxidation does not affect the PL intensity, which demonstrates that the band offsets between InP and ZnS provide the fine confinement of charge carriers. Thus the electrons cannot approach to the surface of InP/ZnS nanocrystals, and the PL property is insensitive to the surface changes when the ZnS shell was thick. However, when the thickness of ZnS shell decreases due to the formation of the oxide layer, the electrons can reach the surface because the electron wave function extends to the shell and to the nanocrystal surface,^{26, 27} and as a result, the QY decreased. InAs/ZnSe nanocrystals with different shell thickness were obtained by removing aliquots of the reaction mixture at different time during the growth of ZnSe shell (the moments when the reaction mixture is reheated to 220 °C, the reaction mixture was maintained at 220 °C for 30 min and 1 hour).

The evolutions of these InAs/ZnSe nanocrystals are shown in Figure 6. The formation of ZnSe shell on InAs nanocrystals improved the QY, which behaves a function of shell thickness. The thicker ZnSe shell led to higher QY. For the thinnest ZnSe shell (Figure 6, top row), the PL intensity and QY increased monotonously accompanied with successive blue-shift of absorption and PL peaks. These evolutions are also due to formation of oxide

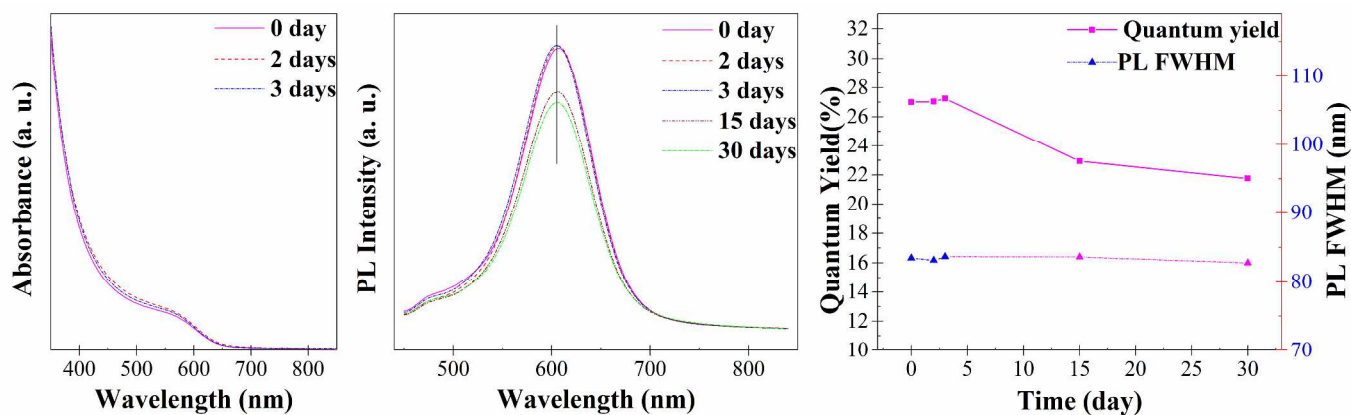


Figure 5. Temporal evolutions of absorption (left) and photoluminescence spectra (middle), photoluminescence FWHM and quantum yield (right) of colloidal InP/ZnS core/shell nanocrystals.

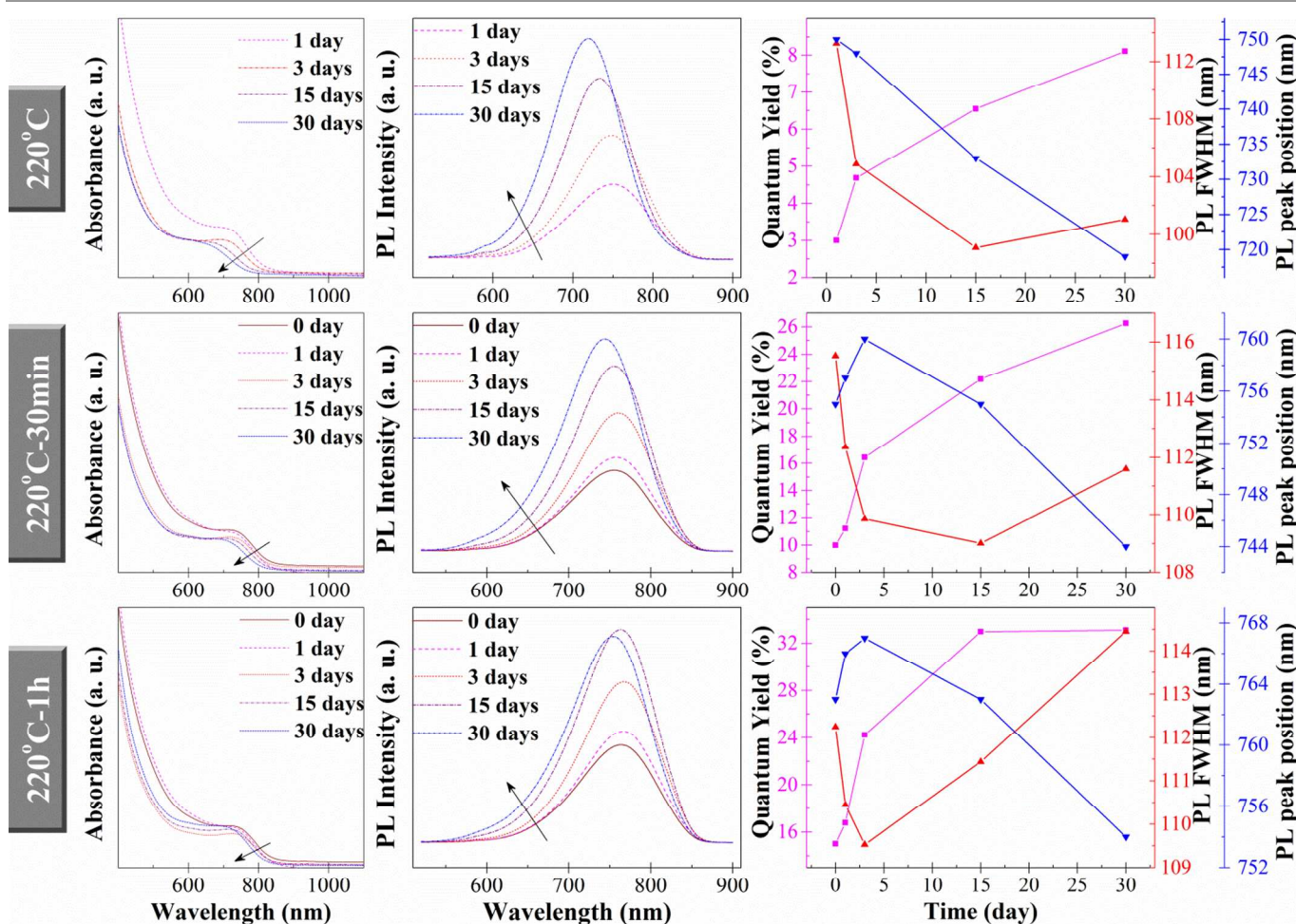


Figure 6. Temporal evolutions of absorption (left) and photoluminescence spectra (middle), quantum yield (■), photoluminescence FWHM (▲) and photoluminescence peak position (▼) (right) of colloidal InAs/ZnSe core/shell nanocrystals with different ZnSe shell thickness. (Top row: colloidal InAs/ZnSe core/shell nanocrystals when the reaction mixture was just heated to 220 °C; Middle row: colloidal InAs/ZnSe core/shell nanocrystals when the reaction mixture was maintained at 220 °C for 30 min; Bottom row: colloidal InAs/ZnSe core/shell nanocrystals when the reaction mixture was maintained at 220 °C for 1 hr.)

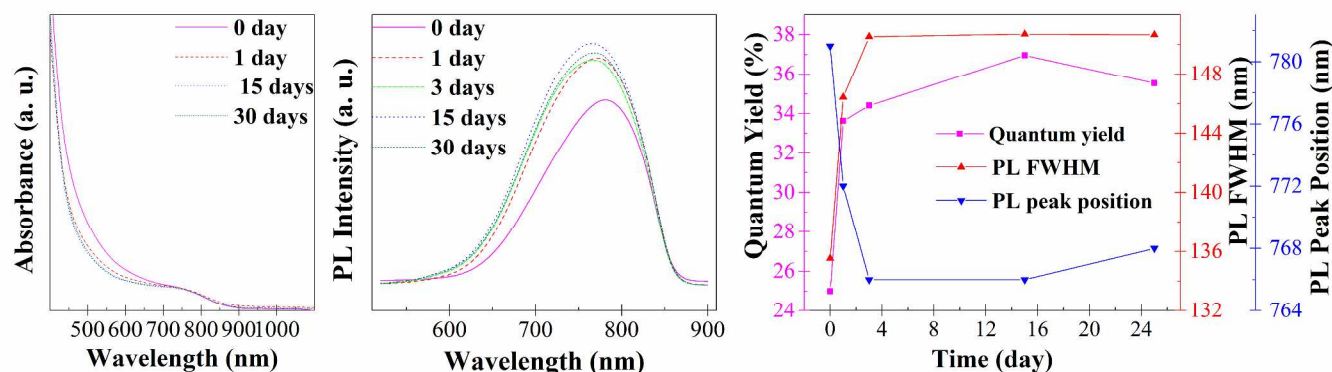


Figure 7. Temporal evolutions of absorption (left) and photoluminescence spectra (middle), quantum yield, photoluminescence FWHM and photoluminescence peak position (right) of colloidal InAs/ZnSe/ZnS core/shell1/shell2 nanocrystals.

layers, but the effect is different from that of InAs core nanocrystals. Because the ZnSe shell is very thin, the oxide layer of ZnSe is adjacent to the surface of InAs core, thus the oxide layer may provide fine surface passivation which resulted in increase of QY. The increase of thickness of the oxide layer reduced the size of core/shell nanocrystals which led to stronger confinement of charge carriers. Consequently, the absorption and PL peaks of InAs/ZnSe nanocrystals shifted to higher energy (shorter wavelength) gradually due to quantum confinement effect.²⁸ The surface oxidation resulted in different change in the PL FWHM which decreased first and then increased. As the shell thickness increased, the QY and PL FWHM showed similar evolutions, while the absorption spectra and the PL peak position showed less change. The change of nanocrystals with thicker shells is much smaller than that of nanocrystals with thinner shells. The sensitivity of InAs/ZnSe nanocrystals to surface states is in accordance with previous observations on core/shell nanocrystals with InAs cores.²⁹

In order to limit the access of electrons to nanocrystal surface, we grew a shell with a broader band gap (ZnS) on InAs/ZnSe nanocrystals. As a result, the QY increased to 25% from 15%. The evolutions of InAs/ZnSe/ZnS nanocrystals are shown in Figure 7. The core/shell1/shell2 nanocrystals are still sensitive to the surface oxidation. Obviously, the evolutions are much faster in the first 3 days than in the next 22 days, and it is faster than that of InAs/ZnSe

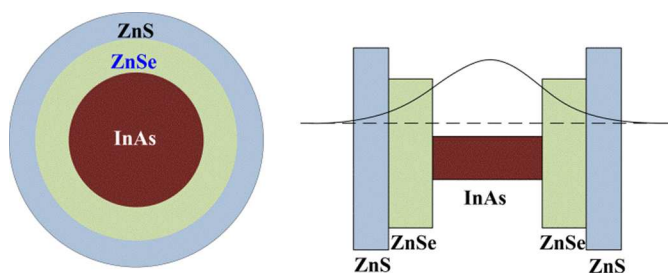


Figure 8. Structure of InAs/ZnSe/ZnS nanocrystals and schematic distribution of the electron wave function in the core/shell1/shell2.

nanocrystals. Interestingly, the QY of the InAs/ZnSe/ZnS nanocrystals decreased a little at the 30th day compared to that when they were stored for 15 days, and this decrease can be attributed to strong surface oxidation. These evolutions demonstrated that the two

conduction band offsets formed in core/shell1/shell2 nanocrystals still could not confine electrons completely inside the nanocrystals due to the extremely small electron effective mass in InAs ($0.027m_e$, m_e is the mass of free electron³⁰).³¹ Structure of InAs/ZnSe/ZnS nanocrystals and schematic distribution of the electron wave function in the core/shell1/shell2 are illustrated in Figure 8. The surface oxidation rate of InAs/ZnSe/ZnS nanocrystals is faster than that of InAs/ZnSe nanocrystals which may be attributed to higher probability of contact with O_2 due to larger surface area of InAs/ZnSe/ZnS nanocrystals (larger nanocrystal size). In consideration of the probability of contact with O_2 , the evolutions of InAs/ZnSe nanocrystals with thick shell, which shows the trend of decrease in QY at the 30th day (Figure 6), confirm larger surface area results in faster oxidation rate.

4. Conclusions

In conclusion, surface oxidation substantially affects the optical property of nanocrystals. The slight oxidation eliminates the surface dangling bonds and leads to PL enhancement while the nanocrystal size is not affected. The strong surface oxidation forms an oxide layer which results in reduction in PL and nanocrystal size. During the storage of 30 days, the InP-zinc stearate nanocrystals showed a very slow rate of surface oxidation and only the slight surface oxidation occurred. On the contrary, the InAs and InAs-zinc stearate nanocrystals showed a much faster surface oxidation rate and only the strong surface oxidation was observed in the 30 days. The diametrically opposed evolutions between InAs and InP nanocrystals is due to their different chemical properties. For the core/shell nanocrystals, the electron wave function extends to shell and to nanocrystal surface, and the maximum length the electron extends to the shell is determined by the electron effective mass in the core and the band offsets between the core and shell materials. The as-synthesized InP/ZnS nanocrystals showed the fine stability in the first few days when the electrons could not approach to the core/shell nanocrystal surface. However, the strong surface oxidation reduced the shell thickness of InP/ZnS core/shell nanocrystals, resulting in that the electrons reach the surface, and thus the PL is sensitive to the surface oxidation. For the core/shell nanocrystals with InAs cores, the InAs/ZnSe nanocrystals with different shell thickness and the

InAs/ZnSe/ZnS nanocrystals were all sensitive to surface states, because the electron could reach the surface of the core/shell and core/shell1/shell2 nanocrystals due to the extremely small electron effective mass in InAs. Consequently, these core/shell nanocrystals showed PL enhancement because of the slight surface oxidation and PL reduction due to the strong surface oxidation. The surface oxidation rate depends on nanocrystal size which determines the surface area and thus the probability of contact with O₂. Generally, due to the surface oxidation, the optical stability of semiconductor nanocrystals depends on the atmosphere where they are stored, nanocrystal size, and may also depend on the methods by which the nanocrystals are synthesized.

Acknowledgements

This work was partially supported by the National Natural Science Foundation of China (NSFC Grand Nos. 60576006 and 51302096), the Fundamental Research Funds of Wuhan City (No. 2013060501010163), and the Fundamental Research Funds of Huazhong University of Science and Technology (No. 2011QN003). The authors thank Ms Chen Xia and the Analytical and Testing Center of Huazhong University of Science and Technology for the help on measurements.

Notes and references

- 1 J. Ziegler, S. Xu, E. Kucur, F. Meister, M. Batenschuk, F. Gindele and T. Nann, *Adv. Mater.* 2008, **20**, 4068-4073.
- 2 N. Tessler, V. Medvedev, M. Kazes, S. Kan and U. Banin, *Science* 2002, **295**, 1506.
- 3 M. C. Schlamp, X. G. Peng and A. P. Alivisatos, *J. Appl. Phys.* 1997, **82**, 5837.
- 4 N. P. Gaponik, D. V. Talapin and A. L. Rogach, *Phys. Chem. Chem. Phys.* 1999, **1**, 1787.
- 5 J. Schafer, J. P. Mondia, R. Sharma, Z. H. Lu, A. S. Susha, A. L. Rogach and L. J. Wang, *Nano Lett.* 2008, **8**, 1709.
- 6 M. Kazes, D. Y. Lewis, Y. Ebenstein, T. Mokari and U. Banin, *Adv. Mater.* 2002, **14**, 317-321.
- 7 J. S. Steckel, S. Coe-Sullivan, V. Bulović and M. G. Bawendi, *Adv. Mater.* 2003, **15**, 1862-1866.
- 8 M. T. Harrison, S. V. Kershaw, M. G. Burt, A. L. Rogach, A. Kornowski, A. Eychmuller and H. Weller, *Pure Appl. Chem.* 2000, **72**, 295.
- 9 X. Michalet, F. F. Pinaud, L. A. Bentolila, J. M. Tsay, S. Doose, J. J. Li, G. Sundaresan, A. M. Wu, S. S. Gambhir and S. Weiss, *Science* 2005, **307**, 538.
- 10 U. Resch-Genger, M. Grabolle, S. Cavaliere-Jaricot, R. Nitschke and T. Nann, *Nat. Methods* 2008, **5**, 763.
- 11 N. Myung, Y. Bae and A. J. Bard, *Nano Lett.* 2003, **3**, 747.
- 12 M. Jones, J. Nedeljkovic, R. J. Ellingson, A. J. Nozik and G. Rumbles, *J. Phys. Chem. B* 2003, **107**, 11346.
- 13 S. R. Cordero, P. J. Carson, R. A. Estabrook, G. F. Strouse and S. K. Buratto, *J. Phys. Chem. B* 2000, **104**, 12137.
- 14 K. Yu, B. Zaman, S. Singh, D. Wang and J. A. Ripmeester, *Chem. Mater.* 2005, **17**, 2552.
- 15 J. Ma, J.-Y. Chen, Y. Zhang, P.-N. Wang, J. Guo, W.-L. Yang and C.-C. Wang, *J. Phys. Chem. B* 2007, **111**, 12012.
- 16 C. Carrillo-Carrión, S. Cárdenas, B. M. Simonet and M. Valcárcel, *Chem. Commun.* 2009, **35**, 5214.
- 17 Q. Dai, Y. Wang, Y. Zhang, X. Li, R. Li, B. Zou, J. Seo, Y. Wang, M. Liu and W. W. Yu, *Langmuir* 2009, **25**, 12320.
- 18 R. Xie, D. Battaglia and X. Peng, *J. Am. Chem. Soc.* 2007, **129**, 15432.
- 19 R. Xie and X. Peng, *Angew. Chem. Int. Ed.* 2008, **47**, 7677-7680.

- 20 (a) J. B. Zhang and D. L. Zhang, *Chem. Mater.* 2010, **22** (4): 1579; (b) J. B. Zhang and D. L. Zhang, *CrystEngComm*, 2010, **12**, 591.
- 21 A. A. Guzelian, J. E. B. Katari, A. V. Kadavanich, U. Banin, K. Hamad, E. Juban and A. P. Alivisatos, *J. Phys. Chem.* 1996, **100**, 7212.
- 22 L. Li and P. Reiss, *J. Am. Chem. Soc.* 2008, **130**, 11588.
- 23 L. Li, M. Protière and P. Reiss, *Chem. Mater.* 2008, **20**, 2621.
- 24 S. Xu, J. Ziegler and T. Nann, *J. Mater. Chem.* 2008, **18**, 2653.
- 25 J. B. Zhang and D. L. Zhang, *CrystEngComm* 2010, **12**(2): 591.
- 26 X. Peng, M. C. Schlamp, A. V. Kadavanich and A. P. Alivisatos, *J. Am. Chem. Soc.* 1997, **119**, 7019.
- 27 P. Reiss, M. Protière and L. Li, *Small* 2009, **5**, 154-168.
- 28 A. P. Alivisatos, *J. Phys. Chem.* 1996, **100**, 13226.
- 29 Y. W. Cao and U. Banin, *Angew. Chem. Int. Ed.* 1999, **38**, 3692-3694.
- 30 Y. -S. Kim, K. Hummer and G. Kresse, *Phys. Rev. B* 2009, **80**, 035203.
- 31 Y. Cao and U. Banin, *J. Am. Chem. Soc.* 2000, **122**, 9692.